Quasistatic remanence in Dzyaloshinskii-Moriya interaction driven weak ferromagnets and piezomagnets

Namrata Pattanayak,[1] Arpan Bhattacharyya,[2] A. K. Nigam,[3] Sang-Wook Cheong,[4] and Ashna Bajpai[1,5,*]

[1]*Department of Physics, Indian Institute of Science Education and Research, Dr. Homi Bhabha Road, Pune 411008, India*

[2]*Saha Institute of Nuclear Physics, 1/AF Bidhannagar, Kolkata, India*

[3]*Department of Condensed Matter Physics and Material Science, Tata Institute of Fundamental Research, Dr. Homi Bhabha Road, Mumbai 400 005, India*

[4]*Rutgers Center for Emergent Materials and Department of Physics and Astronomy, Rutgers University, Piscataway, New Jersey 08854, USA*

[5]*Center for Energy Science, Indian Institute of Science Education and Research, Dr. Homi Bhabha Road, Pune 411008, India*

(Received 29 March 2017; revised manuscript received 19 August 2017; published 18 September 2017)

We explore remanent magnetization (μ) as a function of time and temperature, in a variety of rhombohedral antiferromagnets (AFMs) which are also weak ferromagnets (WFMs) and piezomagnets (PzMs). These measurements, across samples with length scales ranging from nano to bulk, firmly establish the presence of a remanence that is quasistatic in nature and exhibits a counterintuitive magnetic field dependence. These observations unravel an ultraslow magnetization relaxation phenomenon related to this quasistatic remanence. This feature is also observed in a defect-free single crystal of α-Fe_2O_3, which is a canonical WFM and PzM. Notably, α-Fe_2O_3 is not a typical geometrically frustrated AFM, and in single crystal form it is also devoid of any size or interface effects, which are the usual suspects for a slow magnetization relaxation phenomenon. The underlying pinning mechanism appears exclusive to those AFMs which either are symmetry allowed WFMs, driven by Dzyaloshinskii-Moriya interaction, or can generate this trait by tuning of size and interface. The qualitative features of the quasistatic remanence indicate that such WFMs are potential piezomagnets, in which magnetization can be tuned by *stress* alone.

DOI: 10.1103/PhysRevB.96.104422

I. INTRODUCTION

The phenomenon of weak ferromagnetism in certain antiferromagnets (AFMs), including the classic case of α-Fe_2O_3, is associated with the experimental observation of a ferromagneticlike spontaneous moment. This feature was initially attributed to a FM impurity phase in an otherwise AFM lattice, such as Fe_3O_4 impurity in α-Fe_2O_3 [1–4]. This controversy was firmly resolved by Dzyaloshinskii in 1958 [1], who proposed a spin canting mechanism that leads to a weak-ferromagnetic-like state, and Moriya [4], who discovered the microscopic origin of this spin canting and its connection with spin-orbit coupling (SOC). This is the celebrated Dzyaloshinskii-Moriya interaction (DMI), of the type $\mathbf{D}(\mathbf{S}_i \times \mathbf{S}_j)$ which is now central to both fundamental and application based trends in contemporary condensed-matter physics. Apart from exotic inhomogeneous spin textures and noncollinear spin systems such as skyrmions, topological insulators, and superconductors, DMI and SOC also bring into the fore the role of antiferromagnetic insulators in spintronics [5–14].

In many of the symmetry allowed weak ferromagnets (WFMs), which include rhombohedral AFMs like α-Fe_2O_3 and $MnCO_3$ and rutile AFMs like NiF_2 and CoF_2, the phenomenon of stress induced moments or piezomagnetism, of the type ($M_i = P_{ijk}\sigma_{jk}$) where σ is stress, was also predicted by Dzyaloshinskii [1]. Experimental observations of such stress induced moments were made by Borovik-Romanov in a variety of WFM/PzM single crystals (SCs) in seminal work spanning from the 1960s to the 1970s (see [15–18]). On the similar lines of magnetoelectricity, wherein a magnetic moment can be created by *electric field* alone—for which Cr_2O_3 is a prototype [19,20]—a magnetic moment from *stress* alone can occur in a piezomagnet (PzM), for which α-Fe_2O_3 is a prototype [19,21,22]. It is also interesting that both Cr_2O_3 and α-Fe_2O_3 are isostructural AFMs but the piezomagnetic moments are observed in α-Fe_2O_3, not in bulk Cr_2O_3. A picture also emerged with a plausible explanation on the microscopic mechanism of PzMs in these systems [23,24].

In some of these WFM/PzM compounds or in their doped versions [25], an unusually slow magnetization relaxation was tracked through the measurement of remanence. This was further seen in ultrathin films of Cr_2O_3 [26], in FM/AFM core shell systems where Cr_2O_3 appeared as an ultrathin surface layer [27] and also when Cr_2O_3 is encapsulated inside carbon nanotubes [28]. These reports pointed towards some features in remanence which appear to be common, especially for AFMs and possibly for WFM/PzM. Most intriguing among these is the ultraslow magnetization relaxation phenomenon, resulting in the observation of a quasistatic remanence with a counterintuitive magnetic field dependence [27,28].

Interestingly, Cr_2O_3 is not a symmetry allowed WFM/PzM but exhibits quasistatic remanence only when it is in an ultrathin form. It is therefore important to systematically explore whether these features intrinsically exist in symmetry allowed WFMs and to investigate the circumstances in which this can appear in systems with altered symmetry conditions, especially

*ashna@iiserpune.ac.in

due to size and interface effects. In addition, what still remains an open question is whether piezomagnetism will always coexist in all WFMs and, if so, what are the footprints of this phenomenon? It is also important to explore possible means to isolate this subtle effect from routine magnetization measurements, wherein all other field dependent processes contribute for any AFM (canted or otherwise) under magnetic field.

In this paper we explore remanence in two rhombohedral AFMs that are symmetry allowed WFM and PzM. This includes α-Fe_2O_3 with Neel transition temperature (T_N) $\sim$ 950 K and $MnCO_3$ with T_N $\sim$ 30 K. Here α-Fe_2O_3 is known to be a pure AFM up to 260 K and a WFM in the temperature range of 260–950 K [1,16]. The temperature at which α-Fe_2O_3 becomes WFM/PzM is also known as the Morin transition, T_M ($\sim$260 K). It is advantageous to have a WFM near room temperature for practical applications. However, the effect is known to be much weaker than $MnCO_3$[1]. We also investigate isostructural compound $FeCO_3$ with T_N $\sim$ 50 K, for which there are conflicting reports in literature about the existence of WFMs and PzMs [1–3,17]. For such cases, size effects may play a prominent role as DMI can be dominant and enhanced at surfaces and interfaces [29].

We study all three samples in the form of nano- and mesoscopic crystals and particles and show a correlation between the structural parameters and the magnitude of pinned moments related to the quasistatic remanence. In case of α-Fe_2O_3, which is also a prototypical PzM near room temperature, we confirm the ultraslow magnetization relaxation in its single-crystal form, thus bringing out that the quasistatic remanence is intrinsic. We also show that this feature can be substantially tuned by size effects, by comparing the magnitude of quasistatic remanence in the single crystal and nanocubes of α-Fe_2O_3.

II. EXPERIMENTAL TECHNIQUES

Microcubes of $MnCO_3$ (length $\sim$ 2–4 μm), nanocubes of α-Fe_2O_3 (length $\sim$ 200 nm), and polycrystalline spheres of $FeCO_3$ (grain size $\sim$ 5–10 nm) have been synthesized following the precipitation and hydrothermal routes [30–32] [Figs. 1(a)–1(c)]. The single crystal of α-Fe_2O_3 has been grown using float-zone technique. Scanning electron microscopy (SEM) images are recorded using the Zeiss Ultra Plus field-emission SEM. All the samples have been characterized using x-ray powder diffraction (XRD) using Bruker D8 Advance with Cu Kα radiation (λ = 1.54056 Å) [33]. Temperature variation of synchrotron XRD from 20–300 K has been conducted in the BL-18 beam line, Photon Factory, Japan. The synchrotron XRD data have been fitted using Rietveld profile refinement. All three samples stabilize in rhombohedral structure and fitting has been done in hex setting. The XRD data along with the Rietveld fittings at a few selected temperatures for each of the samples are shown in Figs. 1(d)–1(f). The refined lattice parameters a and c at room temperature for all three samples are given in Table I. The temperature variations of refined lattice parameters a and c for the samples are shown in the respective insets in Figs. 1(d)–1(f). Here both a and c are normalized with their respective room-temperature value. The magnetization measurements have been carried out by using a superconducting quantum interference device (SQUID) magnetometer, Quantum Design MPMS-XL.

TABLE I. Structural parameters of $MnCO_3$, α-Fe_2O_3, and $FeCO_3$ as determined from the Rietveld analysis of room-temperature x-ray-diffraction data.

Sample	a (Å)	c (Å)	c/a
$MnCO_3$	4.7723(7)	15.611(3)	3.27
$FeCO_3$	4.6678(4)	15.202(1)	3.25
α-Fe_2O_3	5.0087(1)	13.6856(4)	2.73

III. RESULTS AND DISCUSSIONS

Magnetization as a function of temperature (M_{FC} vs T) recorded while cooling in presence of magnetic field H = 1 kOe is presented in Figs. 1(g)–1(i) for all three samples. This is the routinely known field cooled (FC) cycle. The Neel transition temperatures for $MnCO_3$ and $FeCO_3$, as shown in Fig. 1, match well with the respective literature values. For both these samples, the H is applied in the paramagnetic region, prior to the FC cycle. However, for α-Fe_2O_3, the T_N is 950 K and it is marked schematically in Fig. 1(h). This is to indicate that in the case of α-Fe_2O_3 the magnetization data are recorded while cooling from 300 K, which is above its Morin transition temperature (T_M) but below its Neel temperature (T_N). For a single crystal of α-Fe_2O_3, the magnetization (M_{ZFC}) is also recorded in the zero-field cooled (ZFC) state as will be shown in the latter part of the text. These factors have important implications while preparing a remanent state for all these samples considered here.

A. Preparation of the remanent state: FC and ZFC protocol

Our primary tool here is dc magnetization in the remanent state [34–40]. This enables us to track the magnetization relaxation phenomenon and hence pinning potential landscape in all these WFMs. This remanent state is prepared in two experimental protocols, the FC and ZFC states.

In FC protocol, the sample is cooled in a specified magnetic field, H, which is applied much above the T_N (or T_M), and the M_{FC} is recorded while cooling. The H is switched off at 5 K, and thereafter the remanent magnetization (or remanence) is experimentally measured in the $H = 0$ state. This remanence, prepared after a typical FC cycle, is referred to as μ_{FC}. This can be measured either (i) as a function of increasing *temperature* from 5 to 300 K or (ii) as a function of *time* at 5 K.

In the ZFC protocol, employed only for the single crystal of α-Fe_2O_3, the H is applied from below the T_M and M_{ZFC} is measured in the warming cycle, right up to 300 K. Thereafter H is switched off and the corresponding remanence, referred to as μ_{ZFC}, is measured as a function of *time* at 300 K.

We emphasize that in all the subsequent data involving μ presented in this paper the magnitude of $\boldsymbol{H}$ indicated in the plots refers to the magnetic field applied during either the cooling or warming cycle, so as to prepare a remanent state. This remanence (μ_{FC} or μ_{ZFC}), the origin of which

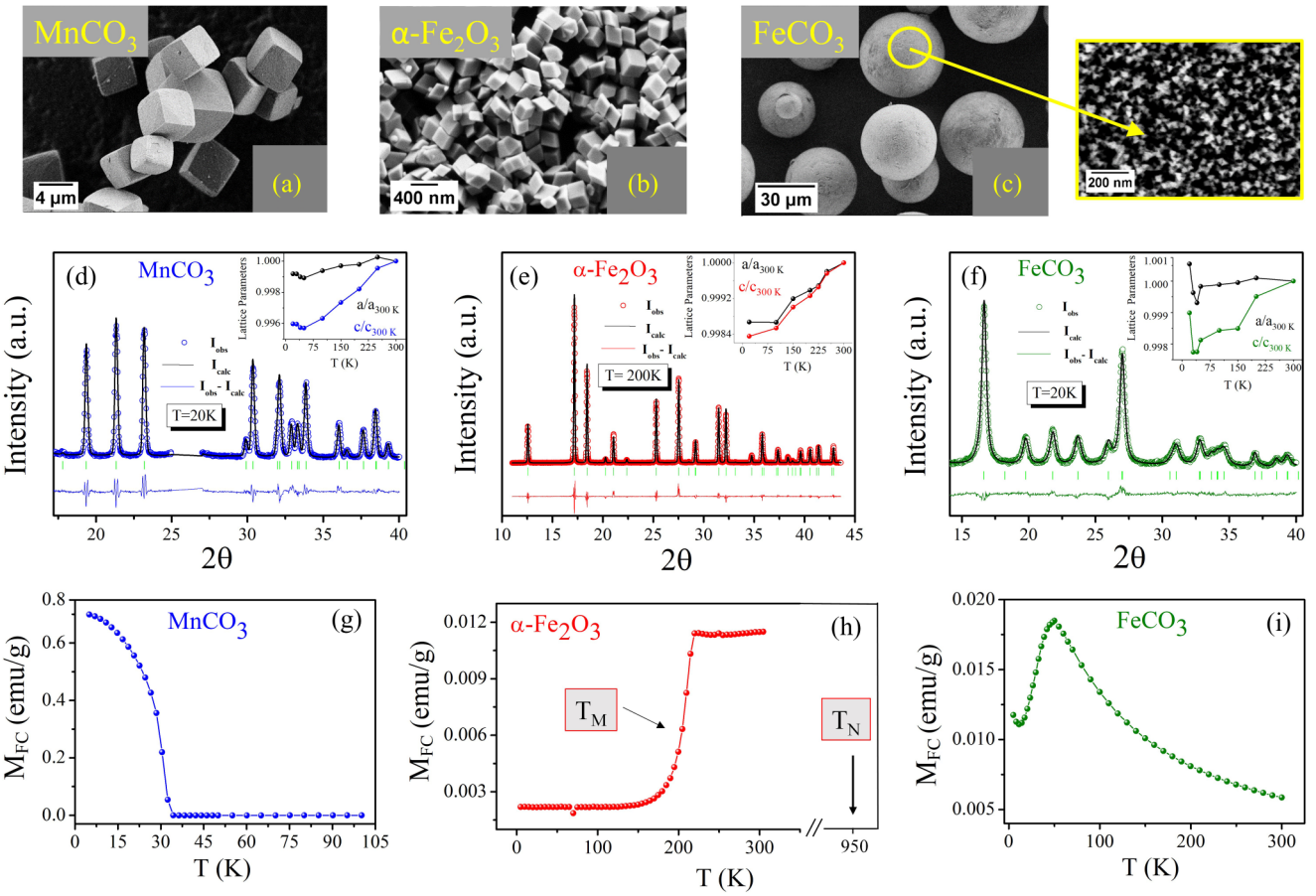

FIG. 1. SEM images of (a) microcubes of $MnCO_3$, (b) nanocubes of α-Fe_2O_3, and (c) $FeCO_3$ spheres with diameter $\sim$20 μm. Each sphere consists of triangular $FeCO_3$ nanoparticles $\sim$5–10 nm. (e, f) Synchrotron XRD data of $MnCO_3$ α-Fe_2O_3 and $FeCO_3$ along with Rietveld fitting. Inset: Best-fit lattice parameters derived from Rietveld profile refinement of I vs 2θ data recorded at different temperatures. (g–i) The magnetization as a function of temperature from 300 to 5 K in presence of $H = 1$ kOe for all three samples. For $MnCO_3$ and $FeCO_3$, the Neel transition temperature is 30 and 50 K, respectively, as evident from (g) and (i), respectively. For α-Fe_2O_3, the Morin transition T_M signifying spin reorientation transition from the WFM to the pure AFM state is around 260 K. The actual Neel transition is around 950 K, shown schematically in (h).

is the subject matter of investigation here, is experimentally measured only after switching *off* the H.

B. Temperature variation of remanence in $MnCO_3$

Figure 2(a) shows M_{FC} vs T (measured while cooling) in presence of $H \sim 100$ Oe (black dots). The magnitude of M_{FC} at 5 K is approximately 0.75 emu/g. After removal of H at 5 K, a part of the magnetization decays instantaneously. However, a significant part of magnetization remains pinned, resulting in the observation of remanence. This remanence (μ_{FC}) shows almost no further decay as a function of time, as long as the temperature is held constant at 5 K. As evident from Fig. 2(a), the magnitude of the μ_{FC} at 5 K is $\sim$0.7 emu/g for this run. On increasing the temperature, μ_{FC} vs T (measured while warming) shows a variation which is qualitatively similar to M_{FC} vs T right up to the T_N as shown in Fig. 2(a) (blue dots). In the paramagnetic tail, the μ_{FC} vanishes, as is expected.

Figure 2(b) shows the same for $H \sim 30$ kOe, for which $M_{FC} \sim 12$ emu/g whereas $\mu_{FC} \sim 10^{-5}$ emu/g at 5 K. Thus the μ_{FC} is vanishingly small for the 30-kOe run. We consider the μ of this magnitude to be roughly arising from the quenched field of the SQUID superconducting magnet, which may be $\sim$5–10 Oe and can vary from run to run [41]. The data contained in Fig. 2 clearly indicate that the magnitude of μ is almost equivalent to that of M_{FC} for lower (cooling) H whereas it is negligible for very high H.

For all the intermediate magnetic fields, the M_{FC} vs T data are plotted in Fig. 2(c) and their corresponding μ_{FC} vs T data are plotted in Fig. 2(d). As is evident from these data, the magnetization increases with increasing H, consistent with a regular AFM behavior. However, the corresponding remanence varies with the strength of the magnetic field in an unexpected way. Here the remanence is first seen to rise with increasing H, up to a critical field. Thereafter it decreases with increase in field and eventually vanishes beyond another critical field.

To clearly bring out the unusual (cooling) field dependence of the μ_{FC}, we compare the magnitude of both M and μ at 5 K. These data points are extracted from different M_{FC} vs T and their corresponding μ_{FC} vs T runs Fig. 2(e). Here M_{FC} is seen to increase with increasing H, as is expected for a regular AFM, whereas the μ_{FC} initially rises with increasing

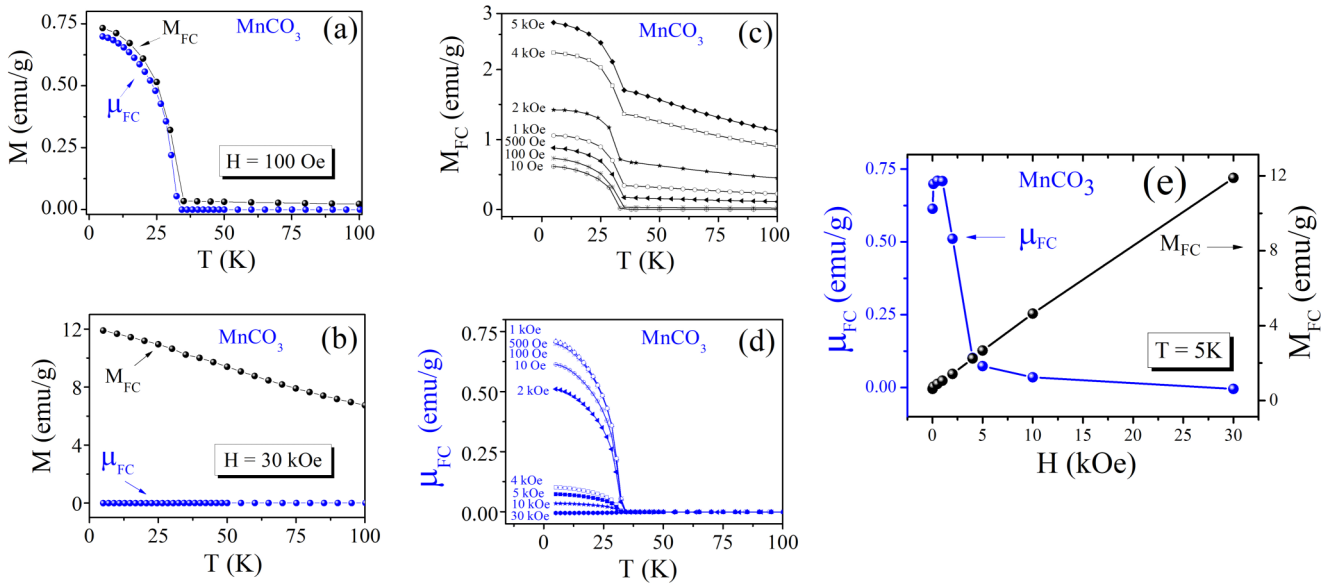

FIG. 2. Black dots in (a) show magnetization measured while cooling ($H = 100$ Oe) and blue dots are corresponding remanence ($H = 0$) measured while warming for the $MnCO_3$ sample. (b) The same for H=30 kOe. (c) M_{FC} vs T at various H depicting regular AFM behavior with M_{FC} rising with rise in H. (d) Corresponding μ_{FC} vs T exhibits strikingly different cooling H dependence. (e) Comparison of the magnitude of M_{FC} (black dots, right axis) and μ_{FC} (blue dots, left axis) at 5 K as a function of (cooling) H for $MnCO_3$.

H, followed by a sharp drop. The μ_{FC} completely vanishes at very high field. The type of field dependence of μ is not expected for either a regular FM or AFM [35–37]. Thus the H dependence of the remanence (blue dots) brings forward a unique functional form, which is not observed in the routine M vs H isotherm (black dots).

C. Remanence in $MnCO_3$: Variation with time

To check the stability of the remanence as a function of time, we also performed relaxation rate measurements. After a typical M_{FC} vs T and subsequent removal of H, we obtained μ_{FC} vs *time*, while the temperature is held constant at 5 K (Fig. 3). These remanence data, obtained for three different cooling fields, again bring forward two distinct magnetization relaxation rates, one of which is ultraslow. We observe that for measurement times of about 2 h the μ_{FC} shows no appreciable decay and this type of remanence can be termed as quasistatic in nature.

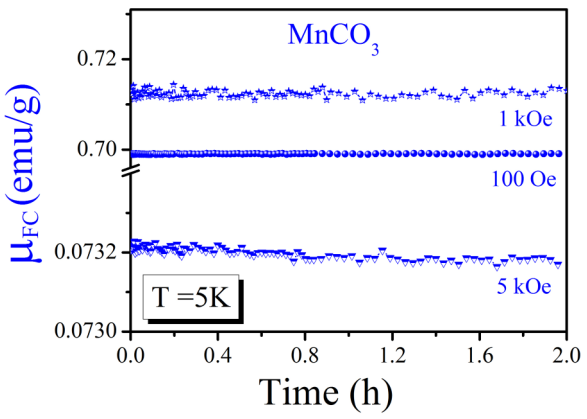

FIG. 3. Remanence as a function of time for three different cooling fields at a fixed temperature of 5 K for $MnCO_3$. These data show that the remanence is almost constant over a time period of 2 h, thus depicting its quasistatic nature.

Consistent with the data presented in Fig. 2(d), magnitude of the μ_{FC} is seen to vary with cooling field H in a way which is not obvious from the routine temperature M-H isotherms. For the chosen cooling fields of 100 Oe, 1 kOe, and 5 kOe, the μ_{FC} values are ~93, 70, and 3% of their corresponding M_{FC} values. These data also indicate that finding an optimum value of the (cooling) magnetic field enables almost all the in-field magnetization to be retained. For instance, the remanence corresponding to the 100-Oe run is 93% of its M_{FC} value. However, even for the run corresponding to 5 kOe, for which the magnitude of remanence is about 3% of its M_{FC} value, the relaxation rate is still ultraslow. Thus the data contained in Fig. 3 confirm presence of the remanence that is quasistatic in nature with ultraslow magnetization dynamics, and exhibits a counterintuitive H dependence [Fig. 2(e)].

D. Remanence and structural parameters in α-Fe_2O_3, $FeCO_3$, and $MnCO_3$

Similar measurements were also conducted for α-Fe_2O_3 and $FeCO_3$ samples. Figures 4(a) and 4(b) display μ_{FC} vs H data at 5 K (extracted from various μ_{FC} vs T runs) for both the samples. These data reveal that the μ_{FC} vs H for each of the samples is strikingly different from corresponding M_{FC} vs H shown on the right axis in each plot. Both the samples exhibit a sharp rise in μ_{FC} as a function of (cooling) H and the peak value of μ is obtained at different critical H for each sample. This rise is qualitatively similar to what is seen for $MnCO_3$ [Fig. 2(e)], though the fall after the peak is not as rapid. Overall, the field dependence of remanence is counterintuitive in all three samples.

In addition, all three samples exhibit two distinct time scales for magnetization decay, one of which is ultraslow

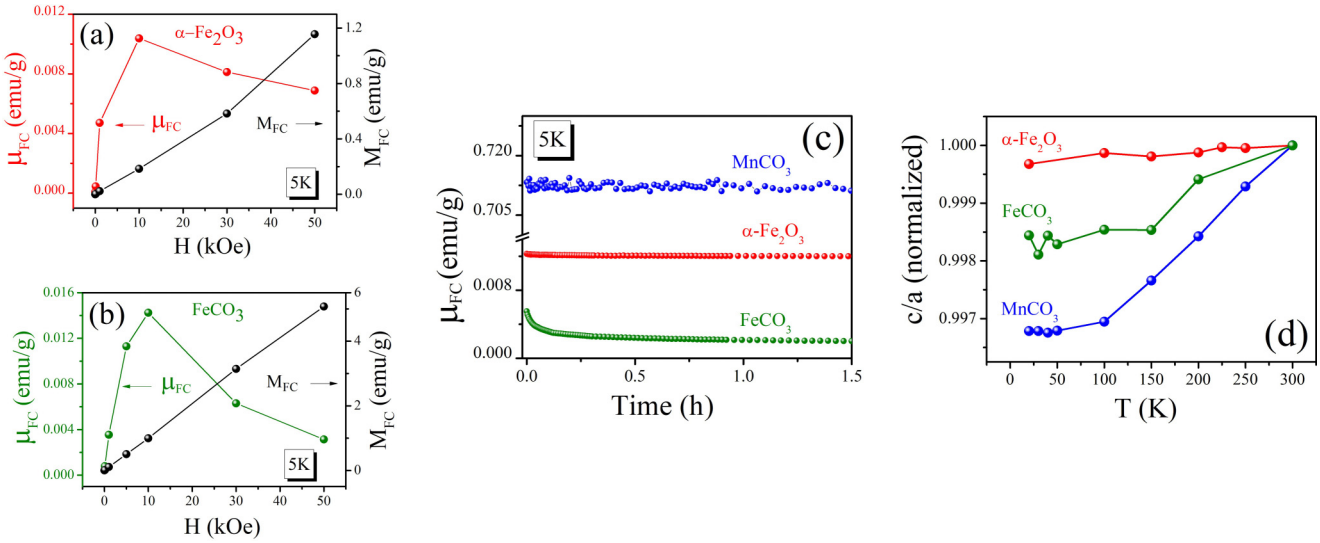

FIG. 4. (a, b) μ_{FC} as a function of (cooling) H for α-Fe_2O_3 and $FeCO_3$, respectively. The corresponding M vs H is shown for each sample in the same graph, indicating the unusual (cooling) field dependence of remanence for both the samples. (c) Comparison of μ_{FC} as a function of $time$ in all three samples. The observation of the quasistatic nature of remanence is unambiguous in case of $MnCO_3$ as well as α-Fe_2O_3. (d) c/a ratio using refined lattice parameters obtained at various temperature from Rietveld fitting of synchrotron XRD data. The c/a ratio has been normalized with its value at 300 K.

and can be termed as quasistatic. This slow magnetization relaxation is evident in μ_{FC} vs T measurements as shown in Fig. 4(c). For the sake of comparison, for each sample the remanent state is prepared in a cooling magnetic field of 1 kOe. The magnitude of the remanence is at least an order of magnitude higher for $MnCO_3$ as compared to α-Fe_2O_3. This is also consistent with the earlier observations which indicate that the net FM moment due to spin canting is about an order of magnitude larger in $MnCO_3$ [1].

To correlate the observed features in μ with structural parameters, the temperature variation of a and c lattice parameters is studied. As can be seen from the inset of Fig. 1(d), for $MnCO_3$, both a and c decrease with reducing temperature monotonically till about the T_N, however an expansion in both the lattice parameters is observed just below its AFM transition temperature. In addition, for $MnCO_3$ the lattice parameter c is seen to fall much more rapidly with reducing temperature as compared to a [inset of Fig. 1(d)]. In contrast, for α-Fe_2O_3, the patterns of temperature variation for c and a are quite similar in nature and a slight trend of expansion in both lattice parameters is observed around its WFM region [Fig. 1(e)]. For all three samples, both lattice parameters exhibit a slight anomaly below T_N (or around WFM in the case of α-Fe_2O_3), however the effect is more pronounced for the $MnCO_3$.

Figure 4(d) compares the normalized c/a ratio as a function of temperature for all three samples. This normalization is with respect to the c/a ratio at 300 K for each sample. We find that the c/a ratio shows a more rapid decline with reducing temperature and a clear anomaly is observed in the WFM region for $MnCO_3$. This trend also correlates with the stability and magnitude of the μ, both of which are relatively higher for $MnCO_3$ as compared to α-Fe_2O_3. In case of $FeCO_3$, though the qualitative features in remanence are similar, the morphology of the sample makes its difficult to conclude whether these features are intrinsic or arising due to nanoscaling. In this case, the grain size is of the order of 2–5 nm [Fig. 1(c)]. This situation is similar to what is observed for Cr_2O_3, which is also isostructural with α-Fe_2O_3, but it is not a symmetry allowed WFM in bulk. However, it exhibits slow relaxation and the unusual cooling field dependence of remanence only in ultrathin form [27,28]. Microscopic measurements are needed to confirm the presence of WFMs in such cases, including ultrasmall $FeCO_3$ grains used in this paper.

For the physical mechanism related to the remanence that results in ultraslow magnetization relaxation, a number of phenomena such as the glassy phase, superparamagnetism, defect pinning in a regular FM or AFM, and exchange bias at the FM/AFM interface can be considered. Such phenomena are known to result in slow relaxation with a variety of temporal functional forms [34–39]. However, the mechanism behind the quasistatic remanence and its unusual (cooling) magnetic field dependence in these samples appears to be different from the above-mentioned phenomena. For instance, considering size effects, $MnCO_3$ shows the most robust magnetization pinning at lower fields, as shown in Fig. 3. However, the sample used for magnetization measurements consists of fairly big crystallites (~2–4 μm), therefore it is less likely that the slow relaxation is arising from size reduction or nanoscaling. It is neither a glassy system nor a nanoscale FM which can exhibit superparamagnetic traits. Crystallites are also regular shaped with well-formed facets, therefore the phenomenon of defect pinning leading to ultraslow magnetization relaxation is ruled out. Also, for a regular AFM/FM, the μ should have shown saturation [35] with H, rather than the sharp drop such as seen in Fig. 2(e).

To understand the nature of remanence in an AFM with WFM traits and to confirm if this effect is intrinsic, we also explored it in a SC. For this purpose, we chose a SC of α-Fe_2O_3 as this sample is well known to exhibit a spin reorientation transition from the pure AFM to WFM phase [1].

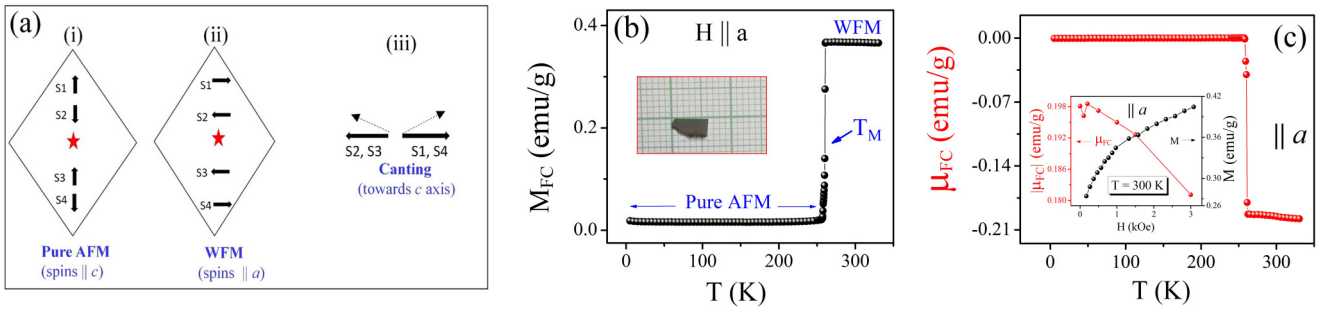

FIG. 5. (a) Schematic of typical spin configurations in the pure AFM (i) and WFM (ii) phase along with the phenomenon of canting (iii). The red star in (i) is the inversion center and the spins point along the c axis in the pure AFM phase. In the WFM phase, spin tilt in the basal plane is shown in (ii). The spin configuration shown in (ii) is necessary for the observation of DMI driven spin canting that results in the WFM phase. (b) M_{FC} vs T for a single crystal of α-Fe_2O_3, with H (1 kOe) parallel to the a axis, exhibiting T_M, the Morin transition, marked as a blue arrow in the figure. Inset: The picture of the α-Fe_2O_3 single crystal. (c) μ_{FC} vs T run corresponding to the M_{FC} vs T run shown in (b). Here the remanence is vanishingly small in the pure AFM region and finite in the WFM region. Inset: μ_{FC} at 300 K along the a axis as a function of various (cooling) H. These data points are extracted from various μ_{FC} vs T runs.

E. Pure AFM and WFM phase: Symmetry considerations

Among the samples considered here, α-Fe_2O_3 is known to be both pure AFM (up to 260 K) and WFM (260–950 K) [1]. Here the pure AFM phase implies that the DMI driven spin canting is not symmetry allowed. As mentioned before, isostructural compound Cr_2O_3, which does not exhibit spin canting, in this context, is a pure AFM phase [1]. For the sake of clarity, the spin configurations in the pure AFM and WFM state are compared in Fig. 5(a). In the pure AFM phase, the spins within the unit cell are arranged along the c axis as shown in Fig. 5(a), configuration (i). Here the red star is the inversion center and the spin configuration can be $S1 = -S2 = S3 = -S4$ as shown in configuration (i). In the WFM state, the spins reorient to the basal plane, arranged in a specific sequence, in which $S1 = -S2 = -S3 = S4$. It is important to note that the unit cell is still AFM, but the spin configuration shown in configuration (ii) is essential for DMI driven spin canting. This $\mathbf{D}(\mathbf{S}_i \times \mathbf{S}_j)$ type of interaction is possible between sublattices associated with antiferromagnetically coupled spins, with the sign of $\mathbf{D}$ consistent with the symmetry considerations discussed in [1–4]. The direction of the net FM moment due to the spin canting is towards the c direction as is shown schematically in Fig. 5(a)(iii). This net FM moment in an otherwise AFM state is responsible for weak ferromagnetism.

The spin configuration shown in Fig. 5(a)(ii) is valid for all the rhombohedral AFMs discussed here, which are symmetry allowed WFMs. For α-Fe_2O_3, the spin reorientation transition from the pure AFM (spins along the c axis) to WFM state (spins along the a axis) occurs at T_M, the Morin transition temperature [1]. Thus α-Fe_2O_3 provides a unique opportunity to probe both the AFM and WFM phase in the same sample, which individually exist in a wide temperature range. In the following, we present results of remanence measurements in the single crystal of α-Fe_2O_3 in both the regions.

F. Remanence in a single crystal of α-Fe_2O_3: Variation with temperature

The main panel of Fig. 5(b) shows M_{FC} vs T for a SC of a α-Fe_2O_3 sample along the a axis. The Morin transition at ~260 K demarcates the two regions, pure AFM and WFM for this sample. From this, we note that the magnitude of M_{FC} is roughly ~0.35 emu/g in WFM region and ~0.015 emu/g in the pure AFM region. After switching off the field at 5 K, corresponding μ_{FC} vs T in the warming cycle is shown in the main panel of Fig. 5(c). The μ_{FC} is found to be negligibly small (10^{-5} emu/g) in the pure AFM region and substantially large in the WFM region (−0.2 emu/g).

Here, the sign of the μ_{FC} is found to be negative with respect to the direction of applied H. From a number of such μ_{FC} vs T data along the a axis, we find that the sign of μ_{FC} at 300 K remains primarily negative and its magnitude shows a slight decrease with increasing magnetic fields [inset in Fig. 5(c)]. It is to be noted that, for obtaining this data, the H during the FC cycle is applied at 300 K, when the sample is in the WFM region. This is unlike the case of $MnCO_3$, where the H can be applied in the paramagnetic region. For obtaining the (cooling) field dependence of remanence unambiguously, such as shown in Fig. 2(e) for $MnCO_3$, it is preferable to apply the H in the paramagnetic region for preparing individual remanent states. However, in the case of α-Fe_2O_3, it is not practically possible to heat the sample above 950 K, after each run. Though the sign of the μ_{FC} along the a axis is not commensurate with the direction applied H while cooling, its magnitude is substantial only in the WFM region.

To check the stability of this remanence as a function of *time*, we conducted relaxation measurements along both the c as well as a axis. Since the direction of the net FM moment is likely to be towards the c axis of the crystal, we particularly checked the stability of μ_{ZFC} as well as μ_{FC} along the c axis as a function of *time*.

G. Remanence in a single crystal of α-Fe_2O_3: Variation with time

In this section we present the relaxation rate of remanence in the pure AFM and WFM phase of α-Fe_2O_3, measured following the FC and ZFC protocol, respectively.

For remanence in the pure AFM region, the H is applied from 300 K and M_{FC} vs T is recorded while cooling (not shown here). The H is switched off at 5 K and the μ_{FC} is measured

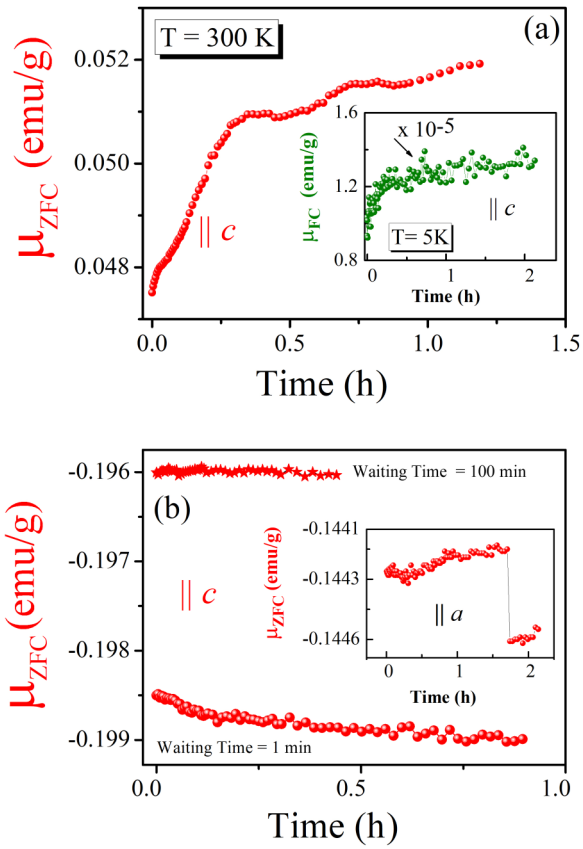

FIG. 6. (a) μ_{ZFC} vs T at 300 K (WFM region) measured along the c axis for the single crystal of α-Fe_2O_3. Inset: μ_{FC} vs T along the c axis at 5 K (pure AFM region). While μ_{FC} is negligibly small in the pure AFM region, it is substantially large (at least by a few orders of magnitude) in the WFM region. (b) μ_{ZFC} vs T measurements parallel to the c axis for a waiting time of 100 min (red stars) and 1 min (red dots). Inset: μ_{ZFC} vs T parallel to the a axis showing a discrete jump.

as a function of time. This is shown in the inset of Fig. 6(a). These data further confirm that the remanence is negligible in the pure AFM region $\sim 10^{-5}$ emu/g [inset of Fig. 6(a)].

For preparing the remanent state in the WFM region, the H is applied from below the T_M and M_{ZFC} vs T is recorded while warming, right up to 300 K (not shown here). At 300 K, the H is switched off and μ_{ZFC} is measured as a function of time [main panel, Fig. 6(a)]. Here, the remanence is positive and is commensurate with the direction of H applied during the ZFC cycle. Thus the remanence is substantial in magnitude in the WFM region and it is also fairly stable in time.

However, from a number of μ_{ZFC} vs time cycles in positive H, we observe that the magnitude of μ_{ZFC} in the WFM region varies from 0.05 to 0.2 emu/g but its sign primarily remains negative. This anomaly appears only in the remanence measurements but not in the regular in-field measurements such as shown in Fig. 5(b). However, such ambiguity with sign has also been observed in the sign of stress induced moments in some WFM/PzM on repeated cooling [15]. The reason for such ambiguity in the case of remanence (which does not appear in regular *in-field* magnetization) is also discussed in the latter part of the text. We also note a slight variation (5%) in the magnitude of μ, from run to run, for the same (cooling) magnetic field. These anomalies are also seen to appear only in the WFM region.

Interestingly, we also observe a slight trend of rise ($\sim$ a few percent of total remanence) in μ_{ZFC} vs time data, as shown in Fig. 6(a). The overall relaxation data appear to be a sum of both time decay as well as time rise of the remanence. This indicates that on application of H (while preparing the remanent state) the moments continue to reorient slowly in the presence of H, and on the removal of H the time decay is ultraslow as well. This also indicates that the total time span in which the H is on for preparing a particular remanent state is also an important parameter. This could also be responsible for variations in the magnitude of the remanence, as observed here. This result prompted us to perform *waiting time* dependence, usually employed for glassy systems [38].

For waiting time runs, two remanent states are prepared using the same (cooling) magnetic field. In the first case, H =1 kOe is applied in the ZFC protocol, from below the T_M, and the sample is heated to 300 K. At 300 K the magnetic field was kept on for a waiting time of 1 min, prior to finally switching it off for the remanence measurements. The second remanent state is prepared following exactly the same protocol, however this time H = 1 kOe is kept on for a waiting time of 100 min, prior to switching it off. These μ_{ZFC} vs T data parallel to the c axis are presented in the main panel of Fig. 6(b), for 1-min (dots) or 100-min (stars) waiting time, respectively. These data clearly indicate that the magnitude of the remanence also changes with the total time span of the H applied for preparing a particular remanent state. This also explains the slight differences in the magnitude of remanence from run to run. The inset shows the same for μ_{ZFC} parallel to the a axis after 100 min of waiting time. Along the a axis, the magnetization relaxation is ultraslow and occasionally discrete jumps in remanence are observed, though the change is less than 1% . However, the remanence continues to exhibit quasistatic nature.

These anomalies which exist in the remanent state are not observed in routine M vs T measurements. α-Fe_2O_3 is not a frustrated AFM and, in the single crystal form, size and interface related phenomena cannot account for the waiting time effects and ultraslow magnetization dynamics. From the observation of quasistatic remanence in a single crystal, together with similar features observed in $MnCO_3$, we conclude that the ultraslow magnetization dynamics can be taken as indicative of the presence of a WFM. This ultraslow dynamics also appears to be associated with the microscopic details of the AFM domain which turns WFM due to spin canting.

H. Quasistatic remanence and DMI driven spin canting

Considering the microscopic reason for quasistatic remanence (that leads to the ultraslow magnetization dynamics as observed here) in these systems, we recall the details of magnetic structure in all these compounds. The spin arrangement shown in Fig. 5(a)(ii) is essential for the observation of WFMs. This should also limit the possible ways in which an AFM domain can exist in the WFM region. For a regular AFM, on the application of the H, the induced magnetization is driven by the Zeeman energy and the magnetocrystalline anisotropy. However, the additional factor in WFMs will include response

from *spontaneously* canted spins, related to the DMI as well. On removal of H, the reversal of the WFM domain will have to be accompanied by the reversal of the AFM moment which is energetically unfavorable [15]. Once an AFM domain with spin canting is formed, guided by a cooling H applied from above the AFM to PzM transition, it is energetically unfavorable for these domains to relax, when the H is removed. This feature is only observed up to a critical value of H which can vary depending on the sample, as is observed here [Figs. 3 and 4(a)]. Beyond a critical H, the magnetization dynamics is driven by Zeeman and magnetocrystalline anisotropy. The magnetization relaxation in this case is much faster, similar to what is observed for a normal AFM. However, below this critical field strength, the WFM domain configuration is guided by the sign of the H field, when it is applied from $T >> T_N$. When the H is applied in the WFM region, the spins are already spontaneously canted. This also explains the ambiguity with sign, as observed in the case of α-Fe_2O_3.

For further confirming that the ambiguity with sign is related to spontaneous spin canting related with DMI and not arising due to measurement related artifacts, we revert back to $MnCO_3$ which has a $T_N \sim 30$ K and H can be applied in the paramagnetic region. Figure 7 shows M_{FC} vs T data recorded while cooling from above T_N, down to 5 K, in the presence of $H = +100$ Oe (blue dots). At 5 K the H is switched off and the quasistatic remanence is observed, which is positive in magnitude as the WFM domain configuration is already guided by the $H = +100$ Oe. Temperature still held at 5 K, we again apply $H = -100$ Oe and subsequent to this the M vs T is measured in the warming cycle (Field Heating cycle) in the presence of $H = -100$ Oe. As is evident from the data shown in Fig. 7, once pinned in the WFM state from above T_N by a positive H, the negative field

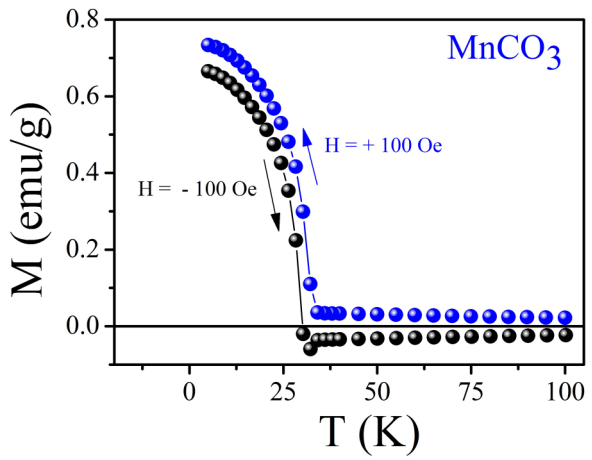

FIG. 7. M vs T recorded while cooling in presence of $H = +100$ Oe (blue dots). At 5 K, $H = +100$ Oe is removed and $H = -100$ Oe is applied while the temperature is held constant at 5 K. Subsequently M vs T in presence of $H = -100$ Oe is again recorded in the warming cycle (black dots). The measured magnetization is basically the remanence prepared during the previous cooling cycle. Since the sample is already in the WFM state, the presence of $H = -100$ Oe is not sufficient to rotate the magnetization. The robustness of the pinned moment, which leads to quasistatic remanence, for $MnCO_3$ is evident from these data.

cannot change the sign of the pinned moment and therefore the sign of remanence. The measured magnetization in the presence of $H = -100$ Oe while warming (black dots) is still positive and clearly a magnetic field applied in the WFM region does not make any difference. Thus the observed magnetization is basically due to the presence of positive remanence, stabilized during the previous ($H = +100$ Oe) FC cycle. These data explain the ambiguity related with the sign of remanence, especially when the H field is applied in the WFM region.

Overall, these data confirm that the quasistatic remanence is observed below a critical value of H in WFMs and related to anisotropic exchange. At higher H, the interplay is between Zeeman and exchange energy, as is usually observed for a regular AFM. The ambiguity related with the sign of μ in a single crystal of α-Fe_2O_3 is related with configuration of AFM domains in which the spins are spontaneously canted due to DMI, even in the absence of H. Cooling or heating in the presence of H leads to stabilization of these canted AFM domains in different configurations, compatible with the interplay of various energy scales involved. This feature again indicates that the net moment related to quasistatic μ is associated with the net FM moment arising due to spontaneous spin canting in an otherwise AFM state.

I. Quasistatic remanence and piezomagnetism

A general consensus in the literature is that a PzM is connected with the transition from the pure AFM to WFM state in an otherwise AFM state and one of the mechanisms that leads to the WFM state is associated with DMI [18]. As mentioned before, the *stress* induced moments have already been experimentally measured in such WFM systems [15–18]. More importantly, the direction of the net FM moment in the WFM phase is seen to coincide with the direction of the PzM [15]. It is also to be recalled that waiting-time effects and ambiguity with sign (similar to what is observed in remanence data for α-Fe_2O_3 with respect to the sign of the applied H) have also been observed in the sign of stress induced moments in WFM/PzM on repeated cooling [15,21].

The data presented in Fig. 7 explain the ambiguity with the sign and the robustness of the pinned moments in the WFM region. The presence of quasistatic remanence also shows that once the WFM domains have been formed, guided by the magnetic field from above the magnetic transition temperature, removal of H (or reversing its sign) does not make any difference. The net FM moment arises due to DMI driven canting; the direction can be manipulated only when the H is applied from above T_N. It is also well known that magnetization reversal in piezomoments would require the reversal of the WFM sublattice which is energetically unfavorable [17]. In remanence measurements, this phenomenon is manifested in the form of ultraslow magnetization relaxation (and consequently the quasistatic remanence) as observed here. These data presented in Figs. 2–7 connect WFMs and quasistatic remanence. These data also further confirm that the WFM phase is intimately related with the onset of transverse PzMs in rhombohedral AFMs.

We emphasize that the remanence data shown here not only bear a striking similarity with experimentally measured

stress induced moments but also reveal features which are not obvious in routine in-field magnetization data. Thus it appears that the remanence measurements capture the essential physics of DMI driven WFMs better than routine M vs T or M vs H and the onset of quasistatic remanence can be taken as footprints of WFMs and PzMs.

From present data it also appears that ultraslow magnetization dynamics and its unusual magnetic field dependence arise from the WFM and such systems are potential PzMs. The magnitude of the WFM/PzM is further related to lattice parameters, especially the c/a ratio in all these rhombohedral systems. A systematic study of such canonical WFM/PzM such as presented here points towards the footprints of this phenomenon by simple magnetization measurements. It is to be emphasized that the system considered here is AFM with WFM traits. These are not frustrated AFMs or a disordered glassy system or spin glass in the conventional sense, which can exhibit slow relaxation for various other reasons. Therefore it is very interesting to observe ultraslow relaxation in a completely ordered system in which these features are correlated with DMI and SOC.

From our data, it can be concluded that for microcubes of $MnCO_3$ and nanocubes and a single crystal of α-Fe_2O_3 the presence of ultraslow magnetization dynamics is associated with the intrinsic WFM. The temperature variation of remanence data on nanocubes [Fig. 4(a)] and a single crystal of α-Fe_2O_3 [Fig. 5(c)] especially bring out that the magnitude of quasistatic remanence can be significantly tuned by nanoscaling, as also has been observed earlier [27,28]. For $FeCO_3$, data are not sufficient to conclude whether the effect is intrinsic or is arising from the size reduction, as the sample comprises 5–10-nm particles of $FeCO_3$. In such cases, the strain in lattice parameters can also stabilize the WFM phase [26–28], however microscopic measurements are needed to confirm the presence of DMI driven canting. It is to be noted that it is relatively hard to stabilize $FeCO_3$ in the form of macroscopic crystallites for ruling out size effects. However, we are in the process of exploring systematic size effects in $FeCO_3$. We also assert that for systems which are isostructural AFM with α-Fe_2O_3, such as Cr_2O_3 (which is definitely not a symmetry allowed PzM) and $FeCO_3$ (for which there are conflicting reports in the literature), the strain in the lattice parameter arising from size effects is likely to stabilize the WFM/PzM phase [27,28].

IV. CONCLUSION

In conclusion, we explore two rhombohedral antiferromagnets that are weak ferromagnets and observe an ultraslow magnetization dynamics and, associated with this, a very robust magnetization pinning with unusual magnetic field dependence. These features are intimately related to the weak ferromagnetism arising from spin canting. This spin canting is associated with DMI for the rhombohedral antiferromagnets discussed here. Whether a qualitatively similar feature can be observed in other WFMs, in which spins are canted but the origin is not DMI driven, is yet to be explored. From the present set of data, it is confirmed that the quasistatic remanence and its unique magnetic field dependence can be taken as footprints of WFM/PZM systems. This feature is intrinsic in nature and the slow relaxation observed here does not relate with magnetization pinning arising from the glassy phase, magnetocrystalline anisotropy, or routine exchange bias. The DMI in the WFM phase is clearly connected with the possibility of stress induced moments or piezomagnetism. Finally, piezomagnetism, though not as widely explored or utilized as, say, piezoelectricity, can have a variety of applications including those related to FM/AFM interfaces, in which the FM moment can be pinned by a PzM, and the effect should be tunable by stress alone.

ACKNOWLEDGMENTS

The authors thank Sunil Nair (Indian Institute of Science Education and Research, Pune) for SQUID magnetization measurements. A.B. acknowledges the Department of Science and Technology (DST), India for funding support through a Ramanujan Grant and the DST Nanomission Thematic Unit Program. S.W.C. is funded by the Gordon and Betty Moore Foundations EPiQS Initiative through Grant No. GBMF4413 to the Rutgers Center for Emergent Materials. The authors thank the DST and Saha Institute of Nuclear Physics, India for facilitating the experiments at the Indian Beamline, Photon Factory, Japan.

[1] I. E. Dzyaloshinskii, JETP **32**, 1259 (1957).
[2] I. E. Dzyaloshinskii, JETP **33**, 807 (1957).
[3] I. E. Dzyaloshinsky, J. Phys. Chem. Solids **4**, 241 (1958).
[4] T. Moriya, Phys. Rev. **120**, 91 (1960).
[5] U. K. Rossler, A. N. Bogdanov, and C. Pfleiderer, Nature (London) **442**, 797 (2006).
[6] Y. Onose, T. Ideue, H. Katsura, Y. Shiomi, N. Nagaosa, and Y. Tokura, Science **329**, 297 (2010).
[7] M. Z. Hasan and C. L. Kane, Rev. Mod. Phys. **82**, 3045 (2010).
[8] Y. Yamasaki, H. Sagayama, T. Goto, M. Matsuura, K. Hirota, T. Arima, and Y. Tokura, Phys. Rev. Lett. **98**, 147204 (2007).
[9] B. Binz, A. Vishwanath, and V. Aji, Phys. Rev. Lett. **96**, 207202 (2006).
[10] C. L. Kane and E. J. Mele, Phys. Rev. Lett. **95**, 226801 (2005).
[11] J. Sinova and I. Zutic, Nat. Mater. **11**, 368 (2012).
[12] V. Barthem, C. Colin, H. Mayaffre, M. Julien, and D. Givord, Nat. Commun. **4**, 2892 (2013).
[13] I. Gross, L. J. Martínez, J.-P. Tetienne, T. Hingant, J.-F. Roch, K. Garcia, R. Soucaille, J. P. Adam, J.-V. Kim, S. Rohart, A. Thiaville, J. Torrejon, M. Hayashi, and V. Jacques, Phys. Rev. B **94**, 064413 (2016).
[14] J. Gayles, F. Freimuth, T. Schena, G. Lani, P. Mavropoulos, R. A. Duine, S. Blügel, J. Sinova, and Y. Mokrousov, Phys. Rev. Lett. **115**, 036602 (2015).
[15] A. S. Borovik-Romanov, Sov. Phys. JETP **11**, 786 (1960).
[16] A. S. Borovik-Romanov, Zh. Eksp. Teor. Fiz. **38**, 1088 (1960).
[17] V. Andratskii and A. S. Borovik-Romanov, JETP **687**, 1036 (1966).

[18] A. S. Borovik-Romanov, Ferroelectrics **162**, 153 (1994).
[19] R. R. Birss, *Symmetry and Magnetism* (North-Holland, New York, 1964).
[20] D. Halley, N. Najjari, H. Majjad, L. Joly, P. Ohresser, F. Scheurer, C. Ulhaq-Bouillet, S. Berciaud, B. Doudin, and Y. Henry, Nat. Commun. **5**, 3167 (2014).
[21] J. Sandonis, J. Baruchel, B. Tanner, G. Fillion, V. Kvardakov, and K. Podurets, J. Magn. Magn. Mater. **104**, 350 (1992).
[22] S. A. J. Kimber and J. P. Attfield, J. Mater. Chem. **17**, 4885 (2007).
[23] T. G. Phillips, R. L. Townsend, and R. L. White, Phys. Rev. Lett. **18**, 646 (1967).
[24] T. G. Phillips, R. L. Townsend, and R. L. White, Phys. Rev. **162**, 382 (1967).
[25] J. Kushauer, W. Kleemann, J. Mattsson, and P. Nordblad, Phys. Rev. B **49**, 6346 (1994).
[26] S. Sahoo and C. Binek, Philos. Mag. Lett. **87**, 259 (2007).
[27] A. Bajpai, R. Klingeler, N. Wizent, A. K. Nigam, S.-W. Cheong, and B. Büchner, J. Phys.: Condens. Matter **22**, 096005 (2010).
[28] A. Bajpai, Z. Aslam, S. Hampel, R. Klingeler, and N. Grobert, Carbon **114**, 291 (2017).
[29] A. Michels, D. Mettus, D. Honecker, and K. L. Metlov, Phys. Rev. B **94**, 054424 (2016).
[30] M. Lisunova, N. Holland, O. Shchepelina, and V. V. Tsukruk, Langmuir **28**, 13345 (2012).
[31] X. Liu, J. Zhang, S. Wu, D. Yang, P. Liu, H. Zhang, S. Wang, X. Yao, G. Zhu, and H. Zhao, RSC Adv. **2**, 6178 (2012).
[32] X. Liu, H. Wang, C. Su, P. Zhang, and J. Bai, J. Colloid Interface Sci. **351**, 427 (2010).
[33] See Supplemental Material at http://link.aps.org/supplemental/10.1103/PhysRevB.96.104422 for the synthesis details of all three samples along with their respective laboratory XRD data.
[34] S. Mørup and C. Frandsen, Phys. Rev. Lett. **92**, 217201 (2004).
[35] M. J. Benitez, O. Petracic, H. Tüysüz, F. Schüth, and H. Zabel, Phys. Rev. B **83**, 134424 (2011).
[36] M. J. Benitez, O. Petracic, E. L. Salabas, F. Radu, H. Tüysüz, F. Schüth, and H. Zabel, Phys. Rev. Lett. **101**, 097206 (2008).
[37] L. Néel, Rev. Mod. Phys. **25**, 58 (1953).
[38] K. Binder and A. P. Young, Rev. Mod. Phys. **58**, 801 (1986).
[39] J. Mattsson, C. Djurberg, and P. Nordblad, Phys. Rev. B **61**, 11274 (2000).
[40] M. Suzuki, I. S. Suzuki, and M. Matsuura, Phys. Rev. B **73**, 184414 (2006).
[41] In SQUID magnetometers, even in $H = 0$, there can be some residual magnetic field arising from the superconducting coil. The magnitude of this residual field can be 5–10 Oe and its sign can be arbitrary. The vanishingly small value of remanence at $H = 30$ kOe also sets the base line for any artifacts arising from such residual fields.